Theoretical Study of Pyrrolidine: Revised Conformational Energies and Vibrational Assignments

Luis Carballeira,*,† Ignacio Pérez-Juste,‡,§ and Christian Van Alsenoy‡

Departamento de Química Física, Facultad de Ciencias, Universidad de Vigo, 36200 Vigo, Spain, and Department of Chemistry, University of Antwerp (UIA), Universiteitsplein 1, B-2610 Wilrijk, Belgium

Received: October 31, 2001; In Final Form: February 1, 2002

The pseudorotational process of pyrrolidine (PYR) and the conformational preference at the N−H position have been thoroughly reinvestigated by means of ab initio methods. To examine electron correlation effects and basis set dependencies, Hartree−Fock (HF), post-Hartree−Fock (MP2, CC, QCI, and CI) and several density functional (DFT) methods with a large variety of basis sets have been employed. It has been found that both post-Hartree−Fock and DFT methods predict opposed energy differences between the N−H axial and N−H equatorial conformers depending on the size of the basis set. However, according to HF and B3LYP computations with the aug-cc-pVQZ basis set, it could be concluded that the N−H equatorial structure is the most stable conformer of PYR. This prediction is in agreement with the last microwave free jet experiment of Caminati et al. [Caminati, W.; Dell′ Erba, A.; Maccaferri, G.; Favero, P. G. *J. Mol. Spectrosc.* **1998**, *191*, 45]. On the basis of the results obtained, the previously reported electron diffraction data and microwave experiments have been reinterpreted. Finally, a detailed reassignment of the experimental vibrational frequencies of pyrrolidine and its N−D isotopomer has also been performed by means of the scaled quantum mechanical force fields computed at the HF, MP2, and B3LYP levels with the 6-31G** basis set.

Introduction

Five-membered saturated rings can change their conformation passing through different puckered and twisted forms in a process named pseudorotation (Figure 1).[1,2] According to Pople and Cremer, pseudorotation can be described using two coordinates,[3] the puckering amplitude, q, which represents the deviation of the ring from planarity, and the pseudorotational phase angle, ϕ, which indicates the position of the ring in the pseudorotational path. Among saturated five-membered rings, the structure and conformational behavior of pyrrolidine (PYR) have been the object of several experimental and theoretical studies, because pyrrolidine rings are present in molecules of biological interest as peptides and proteins.[4−11] Early thermodynamic studies suggested free or almost free pseudorotation for PYR,[4] but a definitive conclusion about the conformational preferences could not be achieved.[5] Caminati et al. dedicated a lot of effort to the elucidation of the axial−equatorial equilibrium at the N−H position. In their first conventional microwave work,[6] they concluded that the most likely conformation of PYR is the N−H axial envelope form (**E1** in Figure 1), and it was pointed out that the axial−equatorial energy difference could not be estimated because of the weak rotational spectrum of the equatorial form. A subsequent electron diffraction spectrum,[7] supported by HF/4-21G(N*) ab initio calculations, was also assigned to the N−H axial conformation, and a pseudorotational barrier of 1.66 kcal/mol was predicted. More recently and in contrast to their previous studies, Caminati et al.[8] reported the accidental discovery of the N−H equatorial conformer (**E6**) in the rotational free jet spectrum of the pyrrolidine−water adduct and concluded from the study of cooling effects in the jet that the equatorial structure is more stable than the axial one by about 220 cm^{-1}.

With regard to theoretical work, few detailed ab initio studies have been exclusively dedicated to the conformational stability of PYR. By means of HF/6-31G** and MP2/6-31G** geometrical optimizations with imposed symmetrical constraints, Kang et al.[9] reported a pseudorotational barrier of 0.8 kcal/mol and concluded that the MP2 results obtained for the axial conformer were in agreement with the electron diffraction published results. Geidel et al.,[10] with the aid of MP2/6-31G* and B3LYP/6-31G* calculations, assigned the experimental vibrational frequencies to the normal modes of the axial conformer. Carballeira et al.[11] characterized the stationary points on the molecular energy surface using HF, MP2, and MP4 methods. The experimental spectroscopic data were interpreted in terms of a mixture of almost isoenergetic N−H axial envelope and N−H axial twist forms. However, because the computed conformational preferences depended largely on the method and the basis set employed, it was concluded that the question of the axial−equatorial preference at the N−H position would remain open until further calculations were performed.

To complete our previous study and to conciliate the disagreement between the reported theoretical predictions and the last experimental observations, we reinvestigate in this paper the conformational behavior of PYR by means of a variety of theoretical methods, which include the use of large basis sets and different treatments of electron correlation. Particular emphasis is devoted on density functional methods because, in contrast with conventional ab initio calculations, their performance still must be tested for a number of conformational problems.[12] It will be shown that the new high level ab initio results obtained provide a complete and consistent interpretation of the published experimental data. Finally, by means of several

* To whom correspondence should be addressed. e-mail: uviqplco@cesga.es.
† Universidad de Vigo.
‡ University of Antwerp (UIA).
§ On leave from the Universidad de Vigo

10.1021/jp014007u CCC: $22.00
Published on Web 03/20/2002

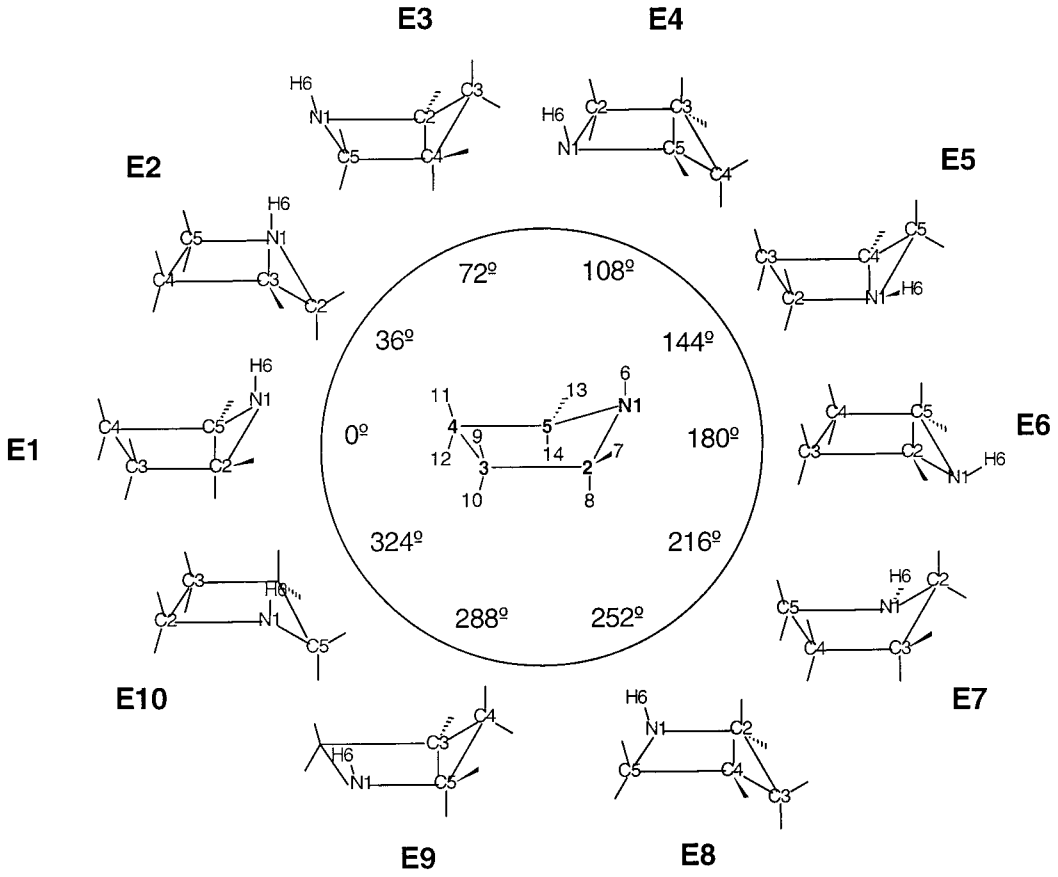

Figure 1. Atom numbering and envelope (**E**) conformations of pyrrolidine along the pseudorotational path. The twist (**T**) conformations are located between adjacents envelope forms.

scaled quantum mechanical force fields, we propose a new normal-mode analysis of the experimental vibrational frequencies of PYR, which allow for a revision of some previous vibrational assignments.

Methods

Ab initio calculations employed in this work include SCF Hartree−Fock (HF),[13] post-Hartree−Fock, and density functional methods. The calculations have been performed with the Gaussian 94 [14] and Gaussian 98 [15] programs. Among post-Hartree−Fock methods, we employed the Møller−Plesset perturbation method at the second order (MP2);[16] the configuration interaction method including all single and double excitations (CISD);[17] the single and double excitations quadratic configuration interaction method (QCISD),[18] also with triple excitations (QCISD(T));[19] and the coupled cluster method including all single and double excitations (CCSD)[20] and, additionally, a quasiperturbative correction for contributions from connected triple excitations (CCSD(T)).[19] To investigate the effect of various density functionals both on the energy and structures of PYR, we have used different combinations between exchange and correlation terms. The exchange term has been considered using the nonlocal gradient corrected exchange functional of Becke (B).[21] The correlation term has been ignored (B-null); treated using the local Vosko, Wilk, and Nusair parametrization[22] (BVWN); or treated according to the gradient corrected functionals of Perdew[23] (BPW91) and Lee, Yang, and Parr[24] (BLYP). Finally, we have also employed the well-known B3LYP functional, which includes a mixture of the Slater, Hartree−Fock, and Becke exchange terms and the LYP correlation functional.[25]

The energy profiles for pseudorotation presented below have been obtained by means of restrained geometrical optimizations of the envelope conformations shown in Figure 1 fixing to zero the torsional angle formed by those four atoms in the same plane for each conformation. HF, MP2, and DFT computations with the 3-21G and 6-31G** basis sets have been used for this purpose. At the same levels, further complete unrestrained geometrical optimizations have been performed for those conformations located in the low-energy regions and for the planar form. The stationary points on the potential energy surface were then characterized by means of their harmonic vibrational frequencies. Additional electron correlated computations have been performed on the stationary points along the pseudorotational path. Thus, CCSD and CCSD(T) single-point energies have been computed on the MP2/6-31G** geometries. QCISD and CISD methods and the 3-21G and 6-31G** basis sets have been employed to reoptimize the geometries of the N−H axial and N−H equatorial envelope structures. To evaluate the effect of the basis set, single-point relative energies have been recomputed using a set of Pople split-valence basis sets [6-311G**, 6-311++G**, and 6-311++G(3df,3pd)], although the largest basis set used for some electron correlated calculations (CC, QCI, and CI) was limited to 6-311++G** by our computational facilities. Additionally, the axial−equatorial energy difference has been reevaluated at the HF and B3LYP levels by means of single-point calculations on the corresponding optimized 6-31G** geometries employing a larger group of basis sets. Thus, we have used the Dunning−Huzinaga double-ζ plus polarization basis set (DZP),[26] the same basis set augmented with diffuse functions (DZP++),[27] and a group of Dunning's hierarchy of correlation-consistent basis sets[28] (cc-

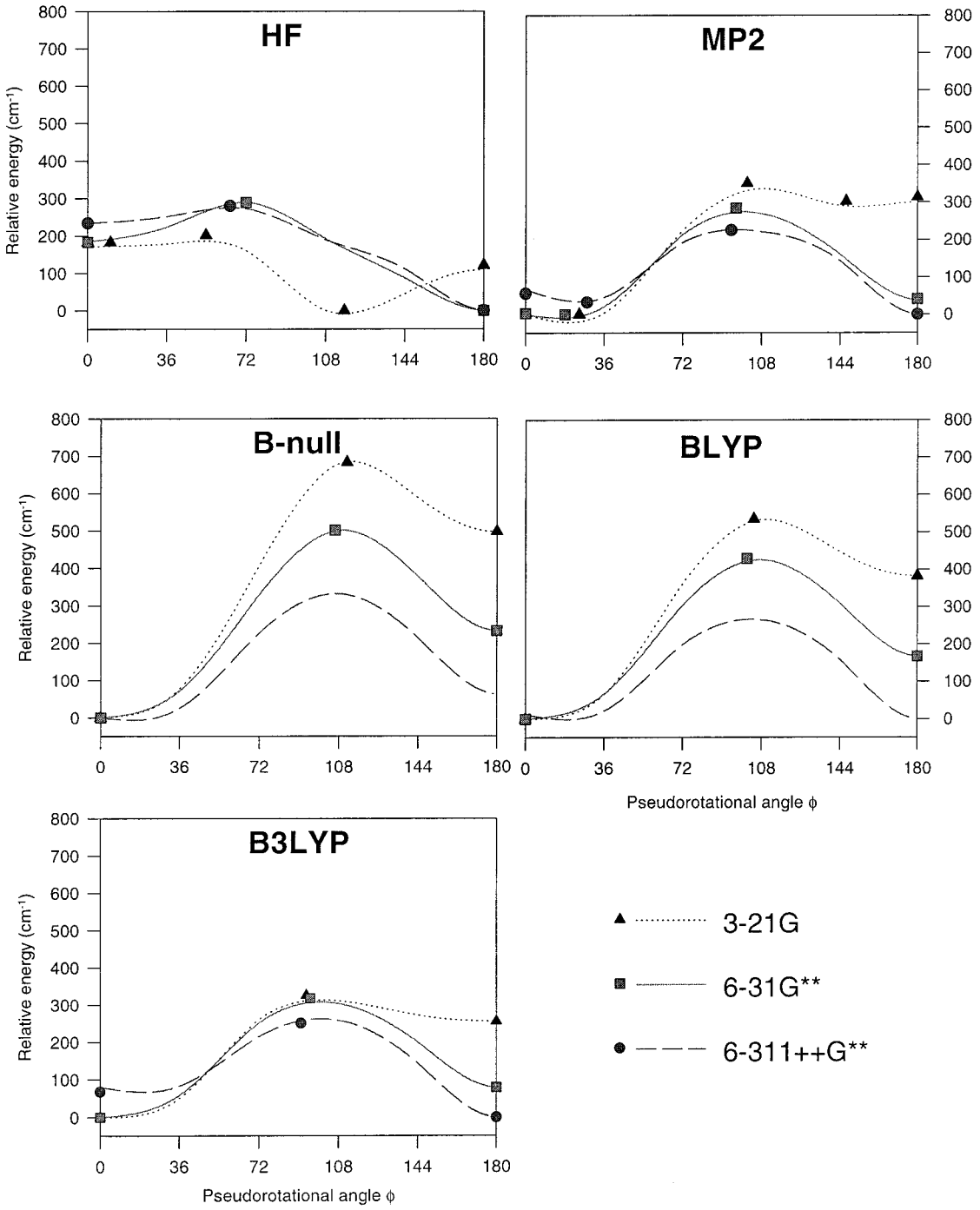

Figure 2. Pseudorotational energy profiles obtained at several computational levels. The symbols represent the stationary points characterized by vibrational analysis.[33,34]

pVDZ, cc-pVTZ, and cc-pVQZ), which were also augmented with diffuse functions[29] (aug-cc-pVDZ, aug-cc-pVTZ, and aug-cc-pVQZ).

The interpretation of the experimental vibrational frequencies have been carried out by using the scaled quantum mechanical (SQM) force fields[30] evaluated at the HF, MP2, and B3LYP levels with the 6-31G** basis set. A suite of programs written at the group of Antwerp has been employed for the vibrational analysis. The analytically computed harmonic Cartesian force constants were transformed into internal coordinates observing local symmetry, defined according to Pulay's method.[31] The force constants were then scaled by a set of scale factors refined in a least-squares iterative process to minimize the difference between calculated and observed frequencies.[30] Finally, the Wilson GF method was employed for the analysis of the vibrational normal modes and its potential energy distribution.[32]

Results and Discussion

Conformational Analysis: The Energy Barrier of Pseudorotation and the Axial/Equatorial Preference at the N−H Position. The pseudorotational energy curves obtained with the procedure cited above are displayed in Figure 2.[33] Because of the symmetry of the pseudorotation of PYR (Figure 1), only the pseudorotational angles between $\phi = 0°$ and 180° are included in the figure. The computed relative energies and the Pople−Cremer puckering coordinates for the stationary points found along the pseudorotational path and for the planar form of PYR are shown in Table 1. These stationary points are also

TABLE 1: Puckering Coordinates (q in Å, ϕ in Degrees) and Relative Energies (in cm^{-1}) of the Stationary Points of Pyrrolidine at Hartree−Fock, Post-Hartree−Fock, and Density Functional Levels

HF/3-21G geometries

	q	ϕ	3-21G	ΔZPE[a]	
E1	0.354	0.00	183	40	(12i)
T1	0.355	10.46	183	46	(16)
T2	0.370	53.79	202	4	(53i)
E4	0.403	116.44	0	0	(78)
E6	0.409	180.00	121	43	(48i)
PL	0.005	0.00	1490	−74	(208i, 202i)

HF/6-31G** geometries

	q	ϕ	6-31G**	6-311G**	6-311++G**	ΔZPE[a]	
E1	0.347	0.00	183	212	234	−6	(33)
E3	0.370	71.91	289	257	275	−73	(70i)
E6	0.413	180.00	0	0	0	0	(62)
PL	0.017	0.00	1688	1752	1685	−116	(232i, 208i)

MP2/3-21G geometries

	q	ϕ	3-21G		
T1	0.380	24.60	0	0	(59)
E4	0.415	101.44	350	−77	(71i)
E5	0.446	146.85	302	−40	(28)
E6	0.455	180.00	313	−53	(30i)
PL	0.049	0.00	1969	−80	(234i, 209i)

MP2/6-31G** geometries

			MP2			CCSD			CCSD(T)				
	q	ϕ	6-31G**	6-311G**	6-311++G**	6-31G**	6-311G**	6-311++G**	6-31G**	6-311G**	6-311++G**	ΔZPE[a]	
E1	0.369	0.00	3	23	62	0	18	55	1	20	17	−21	(31i)
T1	0.373	17.99	0	0	44	0	0	42	0	0	0	0	(42)
T3	0.410	96.36	284	330	224	257	296	209	319	370	223	−80	(70i)
E6	0.452	180.00	41	104	0	26	85	0	87	160	13	−11	(65)
PL	0.041	0.00	2142	2241	2008							−85	(252i, 224i)

QCISD/3-21G geometries

	q	ϕ	3-21G	QCISD(T)/3-21G
E1	0.370	0.00	0	0
E6	0.454	180.00	271	326

QCISD/6-31G** geometries

			QCISD			QCISD(T)		
	q	ϕ	6-31G**	6-311G**	6-311++G**	6-31G**	6-311G**	6-311++G**
E1	0.359	0.00	0	0	48	0	0	0
E6	0.442	180.00	22	72	0	58	139	0

CISD/3-21G geometries

	q	ϕ	3-21G		
E1	0.363	0.00	0		
E6	0.435	180.00	155		

CISD/6-31G** geometries

	q	ϕ	6-31G**	6-311G**	6-311++G**
E1	0.356	0.00	70	58	132
E6	0.429	180.00	0	0	0

B-null/3-21G geometries

	q	ϕ	3-21G	ΔZPE[a]	
E1	0.366	0.00	0	0	(56)
E4	0.416	111.62	683	−121	(84i)
E6	0.464	180.00	497	−58	(61)
PL	0.076	0.00	1875	−144	(221i, 185i)

B-null/6-31G** geometries

	q	ϕ	6-31G**	6-311G**	6-311++G**	ΔZPE[a]	
E1	0.349	0.00	0	0	0	0	(55)
E4	0.395	106.27	501	474	337	−107	(78i)
E6	0.440	180.00	232	210	67	−40	(77)
PL	0.061	0.00	1637	1582	1359	−136	(222i, 187i)

BVWN/3-21G geometries

	q	ϕ	3-21G	ΔZPE[a]	
E1	0.359	0.00	0	0	(61)
E4	0.402	107.09	529	−126	(75i)
E6	0.442	180.00	408	−52	(60)
PL	0.058	0.00	1750	−148	(218i, 191i)

BVWN/6-31G** geometries

	q	ϕ	6-31G**	6-311G**	6-311++G**	ΔZPE[a]	
E1	0.343	0.00	0	0	0	0	(57)
E4	0.383	101.98	408	358	244	−112	(74i)
E6	0.425	180.00	176	128	11	−39	(75)
PL	0.050	0.00	1557	1483	1284	−137	(222i, 191i)

BPW91/3-21G geometries

	q	ϕ	3-21G	ΔZPE[a]	
E1	0.374	0.00	0	0	(53)
E4	0.415	102.33	534	−128	(73i)
E6	0.456	180.00	416	−42	(55)
PL	0.049	0.00	2047	−146	(232i, 202i)

BPW91/6-31G** geometries

	q	ϕ	6-31G**	6-311G**	6-311++G**	ΔZPE[a]	
E1	0.355	0.00	0	0	9	0	(55)
E4	0.396	99.52	437	365	262	−121	(82i)
E6	0.437	180.00	184	103	0	−46	(76)
PL	0.048	0.00	1814	1742	1536	−133	(233i, 200i)

TABLE 1 (Continued)

BLYP/3-21G geometries						BLYP/6-31G** geometries						
	q	ϕ	3-21G	ΔZPE[a]			*q*	ϕ	6-31G**	6-311G**	6-311++G**	ΔZPE[a]	
E1	0.368	0.00	0	0	(53)	**E1**	0.353	0.00	0	0	9	0	(53)
E4	0.410	104.05	534	−123	(77i)	**E4**	0.394	101.38	429	399	275	−114	(76i)
E6	0.452	180.00	382	−43	(58)	**E6**	0.437	180.00	167	126	0	−33	(78)
PL	0.054	0.00	1911	−146	(227i, 196i)	**PL**	0.050	0.00	1750	1674	1451	−138	(230i, 198i)
B3LYP/3-21G geometries						B3LYP/6-31G** geometries						
	q	ϕ	3-21G	ΔZPE[a]			*q*	ϕ	6-31G**	6-311G**	6-311++G**	ΔZPE[a]	
E1	0.364	0.00	0	0	(48)	**E1**	0.351	0.00	0	0	82	0	(35)
T3	0.399	93.50	326	−115	(72i)	**T3**	0.388	95.14	318	272	257	−113	(82i)
E6	0.437	180.00	256	−33	(43)	**E6**	0.428	180.00	79	27	0	−24	(79)
PL	0.035	0.00	1744	−146	(223i, 200i)	**PL**	0.039	0.00	1690	1637	1556	−129	(231i, 202i)

[a] Relative zero point energies (in cm^{-1}). The lowest vibrational frequencies (in cm^{-1}) are shown in parentheses.

represented by the symbols in Figure 2. According to the energy profiles obtained, the description of pseudorotation is strongly influenced by the computational method and by the size of the basis set. At the HF/3-21G and MP2/3-21G levels, the number of stationary points and their positions on the pseudorotational path are clearly different than those obtained with larger basis sets. At the HF/3-21G level, the approximate twist **T1** (ϕ = 10.5°) and **E4** (ϕ = 116.4°) conformations are energy minima and the N−H axial (**E1**, ϕ = 0°) and N−H equatorial (**E6**, ϕ = 180°) envelope structures are transition states. If electron correlation is considered at the MP2/3-21G level, approximate **T1** (ϕ = 24.6°) and **E5** (ϕ = 146.8°) forms are energy minima connected by two **E4** (ϕ = 101.4°) and **E6** transition states. However, the profiles obtained with the DFT methods and the 3-21G basis set are similar to those obtained with larger basis sets, although the barrier height seems to be largely overestimated with B-null/3-21G and BLYP/3-21G computations. These results reinforce the conclusions of our previous study, where we suggested that nonpolarized basis sets are unsuitable for describing the pseudorotational behavior of PYR.[11] The limitations of the nonpolarized basis sets should be particularly taken into account if ab initio calculations are performed on large molecules containing pyrrolidine rings, where the size of the molecules prevents the use of extended basis sets.

The HF, MP2, and DFT pseudorotational energy profiles obtained with larger basis sets (6-31G**, 6-311G**,[33] and 6-311++G**) are quite similar. Thus, the pseudorotation potential is always composed of two low-energy regions around the axial and equatorial forms, separated by an energy barrier in the region around ϕ = 72°−108°. However, significant differences can be observed on the relative energies of the stationary points depending on the theoretical method used (Table 1). At the HF level, the equatorial form is always more stable than the axial conformation. The axial−equatorial energy difference increases slightly with the size of the basis set, until 234 cm^{-1} at the HF/6-311++G** level. If electron correlation is considered at the DFT and MP2 levels, no clear preference at the N−H position is observed. Thus, B-null, BVWN, BPW91, and BLYP methods predict that the axial structure is more stable or essentially isoenergetic to the equatorial conformation, whereas B3LYP/6-311++G** calculations indicate that the equatorial form is around 80 cm^{-1} more stable. At the MP2 level, the equatorial conformer is also predicted to be around 60 cm^{-1} more stable only if the 6-311++G** basis set is used. Remarkably, the vibrational frequencies computed at the MP2/6-31G** level indicate the axial twist form (**T1**, ϕ = 18°) is an energy minimum almost isoenergetic to the axial envelope conformation **E1**, which is characterized as a transition state by vibrational analysis. This particular conformational prediction is not obtained with any DFT method, and the axial form is always characterized as an energy minimum. Because of the flexibility of the ring, small differences are also observed in the conformation at the energy barrier, which is predicted to be an envelope **E3** form (ϕ = 71.9°) at the HF/6-31G** level, a twist **T3** form with MP2/6-31G** (ϕ = 96.3°) and B3LYP/6-31G** (ϕ = 95.1°) methods, and an envelope **E4** form (with ϕ values around 100°) by B-null, BVWN, BPW91, and BLYP computations. It must be also noted that the effect on the axial−equatorial energy differences of the zero-point vibrational energies (ZPE) is almost negligible or tends to stabilize very slightly the equatorial conformation. In contrast, the barrier height to pseudorotation is reduced between 80 and 100 cm^{-1} when ZPE is considered. On the other hand, HF, MP2, and DFT methods agree to indicate that ring inversion through the planar form (**PL**, a second-order transition state) is hindered by a energy barrier between 1300 and 2000 cm^{-1}; therefore, the interconversion between the N−H axial and equatorial forms occurs through the low-energy pseudorotational path. Kang et al.[9] reported a slightly higher energy barrier for this conformational path (around 2100 cm^{-1}), probably because it was obtained by means of restricted MP2/6-31G** geometrical optimization of a perfectly planar structure (q = 0) without further vibrational characterization.

To further analyze the influence of electron correlation and the basis set dependence, we also tested the performance of several post-Hartree−Fock methods, focusing only on the stationary points found on the pseudorotational path. It can be seen from Table 1 that the CCSD and MP2 relative energies are quite similar, and a definitive conclusion about the axial or equatorial predominance cannot be obtained. However, CCSD(T) computations predict that the axial **T1** form is more stable, although the axial−equatorial energy difference obtained with the 6-311++G** basis set is almost negligible (13 cm^{-1}). QCISD and CISD geometrical optimizations of the axial and equatorial forms were also performed with 3-21G and 6-31G** basis sets. The 3-21G results are again clearly different to those obtained with larger basis sets and, as indicated above, should be considered unreliable. QCISD calculations predict opposed axial−equatorial energy differences depending on the basis set employed, and QCISD(T) results indicate that the axial form is preferred, although both forms are of the same energy when the 6-311++G** basis set is used. It must be remarked that only CISD computations using polarized basis sets always predict that the equatorial conformer is more stable (70, 58, and 132 cm^{-1}).

Despite the number of computational methods employed, it cannot be observed a regular dependency of the axial−equatorial energy difference with electron correlation or with the size of

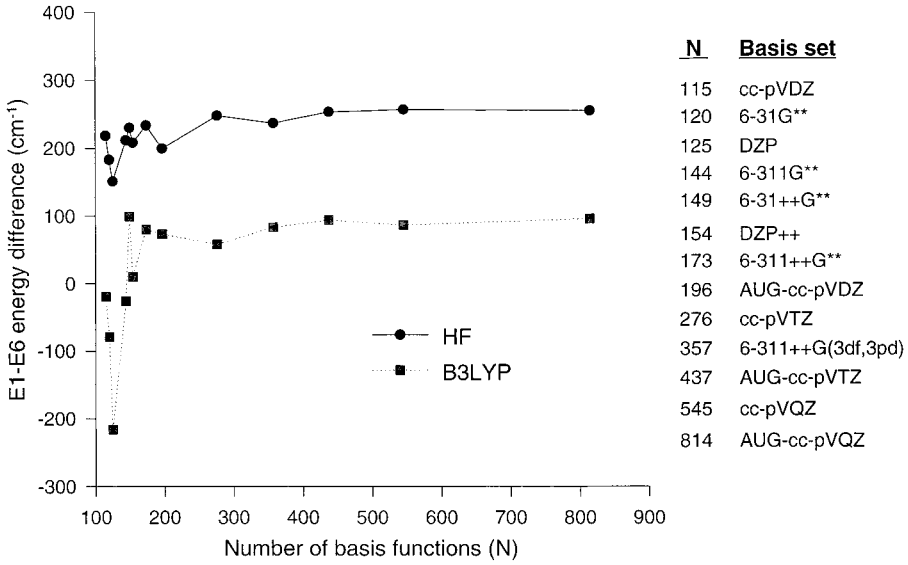

Figure 3. HF and B3LYP energy difference between the axial (**E1**) and equatorial (**E6**) conformers of pyrrolidine obtained with single-point computations on the HF/6-31G** and B3LYP/6-31G** optimized geometries and different basis sets.

TABLE 2: Relative Energies (in cm^{-1}) of the Stationary Points of Pyrrolidine Obtained with the 6-311++G(3df,3pd) Basis Set and the 6-31G Optimized Geometries at Several Computational Levels**

HF		MP2		B-null		BVWN		BPW91		BLYP		B3LYP	
E1	236	**E1**	77	**E1**	0	**E1**	0	**E1**	18	**E1**	15	**E1**	84
		T1	72										
E3	260	**T3**	248	**E4**	307	**E4**	210	**T3**	248	**E4**	252	**E3**	236
E6	0	**E6**	0	**E6**	62	**E6**	4	**E6**	0	**E6**	0	**E6**	0
PL	1676	**PL**	2111	**PL**	1306	**PL**	1222	**PL**	1475	**PL**	1397	**PL**	1469

the basis set, and the conformational preference at the N−H position of PYR is still unclear. Because the size of the electron correlated computations is avoided for the use of larger basis sets, only HF and B3LYP methods could be used for an additional test on the basis set dependence. Thus, HF and B3LYP single-point energies on the 6-31G** optimized geometries were reevaluated with basis sets of increasing size. The largest of the calculations was made with the aug-cc-pVQZ basis set resulting in a total of 1044 primitive Gaussian functions contracted to 814 basis functions. The computed axial−equatorial energy differences for the complete series of basis sets used are represented in Figure 3. Two aspects should be remarked on. On the one hand, the axial−equatorial energy differences computed at the HF and B3LYP levels seem to achieve basis-set convergence. On the other hand, the equatorial conformer is predicted to be more stable when the energy differences achieve convergence. As the results obtained with Pople, Dunning, and correlation-consistent basis sets present the same behavior, it can also be deduced that the basis-set convergence depends mainly on the size of the basis set and not on its nature or quality. The most significant difference between the two sets of calculations is the reduction of the HF equatorial preference from 255 to 96 cm^{-1} because of the electron correlation effects treated with the B3LYP functional.

According to the above, the size of the basis set seems to be crucial to obtain a reliable prediction of the conformational preferences in PYR. Therefore, the HF, DFT, and MP2 relative energies obtained with the 6-311++G(3df,3pd) basis set on the corresponding 6-31G** optimized geometries shown in Table 2 could be considered good estimates for the conformational preferences of PYR. The choice of the basis set is based on a compromise between its computational cost and its good performance, because the HF and B3LYP values obtained with the 6-311++G(3df,3pd) basis set seem to be close to the energy convergence (Figure 3). According to the HF, B3LYP, and MP2 results, the equatorial form is the most stable conformer of PYR, and the axial−equatorial energy difference takes values of about 236, 84, and 77 cm^{-1}, respectively. At the same computational levels, the heights of the pseudorotational barrier are 260, 236, and 248 cm^{-1}, and the energy barriers for axial/equatorial interconversion through the planar form are around 1676, 1469, and 2111 cm^{-1}. On the other hand, the poor agreement between the B3LYP results and those obtained with other density functionals should be also noted, even with the large 6-311++G(3df,3pd) basis set. Thus, the axial form is more stable (62 cm^{-1}) according to Becke's corrected exchange functional results, whereas both axial and equatorial forms are essentially of the same energy if the BVWN, BPW91, and BLYP functional are used.

To summarize, it can be concluded from theoretical calculations with large basis sets that the equatorial structure is the most stable conformer of PYR. Even more, because the axial−equatorial energy difference tends to be reduced because of electron correlation effects, the most likely value for the equatorial predominance could be around 80−100 cm^{-1}, which is in qualitative agreement with the approximate experimental value of 220 cm^{-1} given recently by Caminati et al.[8,34] On the other hand, if electron correlation effects and zero-point energies are considered, the estimated value of the energy barrier for pseudorotation would be around 150 cm^{-1}.

Comparison with Experiment. Vibrational Assignments. Some selected 6-31G** geometrical parameters for the axial and equatorial forms of PYR are shown in Table 3. With regard to the influence of the theoretical method in the computed geometries, it can be observed that most of bond lengths and bond angles do not change significantly from their Hartree−Fock values when electron correlation is considered. Thus, C−C bond distances show positive (QCISD and B3LYP) and negative (MP2 and CISD) deviations from their Hartree−Fock values, with the differences being always smaller than 0.008 Å and the endocyclic N−C−C and C−C−C angles almost invariant with the method employed. On the other hand, the inclusion of electron correlation causes an increase of about 0.01 Å of the N−C bond lengths, which is accompanied by a reduction (about 1−2°) of the C−N−C and H−N−C bond angles. As a

TABLE 3: Selected Geometrical Parameters of the Stationary Points of Pyrrolidine (Bond Lengths in Å, Bond Angles in Degrees)

	HF/6-31G**		B3LYP/6-31G**		MP2/6-31G**			QCISD/6-31G**		CISD/6-31G**		
	E1	E6	E1	E6	E1	T1	E6	E1	E6	E1	E6	exp[7]
N1−C2	1.4568	1.4524	1.4711	1.4654	1.4686	1.4676	1.4634	1.4709	1.4665	1.4600	1.4547	1.469(10)[a]
C2−C3	1.5447	1.5362	1.5537	1.5433	1.5439	1.5365	1.5340	1.5472	1.5381	1.5406	1.5318	1.543(8)
C3−C4	1.5484	1.5495	1.5553	1.5572	1.5465	1.5435	1.5480	1.5500	1.5514	1.5434	1.5444	1.543(8)
C4−C5	1.5447	1.5362	1.5537	1.5433	1.5439	1.5519	1.5340	1.5472	1.5381	1.5406	1.5318	1.543(8)
C5−N1	1.4568	1.4524	1.4711	1.4654	1.4686	1.4711	1.4634	1.4709	1.4665	1.4600	1.4547	1.469(10)
H6−N1	1.0018	0.9996	1.0196	1.0166	1.0181	1.0179	1.0154	1.0171	1.0140	1.0080	1.0057	1.020
H7−C2	1.0839	1.0845	1.0938	1.0951	1.0894	1.0895	1.0900	1.0901	1.0907	1.0838	1.0845	1.090(4)
H8−C2	1.0866	1.0940	1.0976	1.1066	1.0924	1.0929	1.1006	1.0933	1.1009	1.0868	1.0944	1.090(4)
H9−C3	1.0856	1.0837	1.0951	1.0933	1.0904	1.0913	1.0887	1.0916	1.0899	1.0852	1.0835	
H10−C3	1.0847	1.0843	1.0944	1.0935	1.0898	1.0899	1.0892	1.0908	1.0903	1.0844	1.0839	
N1−C2−C3	106.78	102.96	107.17	102.79	106.96	106.06	102.31	107.04	102.57	106.87	102.69	104.6
C2−C3−C4	104.14	104.40	104.12	104.37	104.01	103.47	104.20	104.14	104.31	104.12	104.35	104.9
C3−C4−C5	104.14	104.40	104.12	104.37	104.01	104.16	104.20	104.14	104.31	104.12	104.35	104.9
C4−C5−N1	106.78	102.96	107.17	102.79	106.96	107.70	102.31	107.04	102.57	106.87	102.69	104.6
C5−N1−C2	104.45	105.60	103.67	104.88	102.72	103.04	103.66	103.23	104.04	103.62	104.72	105.2(35)
H6−N1−C2	109.29	112.77	108.14	112.05	107.56	107.25	111.45	107.69	111.37	108.42	112.19	107.0
H7−C2−N1	110.84	110.98	110.67	110.88	110.73	110.82	110.98	110.62	110.87	110.78	111.02	
H8−C2−N1	108.28	112.40	108.06	112.95	107.59	107.82	112.63	107.81	112.56	108.00	112.53	
H8−C2−H7	107.33	107.68	107.30	107.60	107.73	107.92	108.05	107.60	107.97	107.49	107.83	
H9−C3−C2	110.61	110.31	110.65	110.43	110.32	109.39	110.15	110.44	110.24	110.48	110.23	
H10−C3−C2	111.94	111.68	111.96	111.52	112.07	113.13	111.64	111.96	111.62	111.97	111.65	
H10−C3−H9	107.04	107.47	106.96	107.46	107.24	107.44	107.72	107.16	107.61	107.12	107.57	
N1−C2−C3−C4	21.98	25.44	22.15	26.20	23.39	32.26	27.72	22.68	27.09	22.61	26.43	
C2−C3−C4−C5	0.00	0.00	121.45	0.00	0.00	−11.40	0.00	121.45	0.00	0.00	0.00	
C3−C4−C5−N1	−21.98	−25.44	−22.15	−26.20	−23.39	−12.77	−27.72	−22.68	−27.09	−22.61	−26.43	
C4−C5−N1−C2	36.33	43.49	36.28	44.55	38.09	32.81	46.85	37.02	45.81	37.09	44.91	
C5−N1−C2−C3	−36.33	−43.49	−36.28	−44.55	−38.09	−40.47	−46.85	−37.02	−45.81	−37.09	−44.91	
H6−N1−C2−C3	80.52	−167.07	78.35	−166.33	75.23	72.99	−166.83	76.72	−165.89	77.95	−166.84	

[a] Values between brackets correspond to 3σ error limits as defined in ref 7.

consequence of these geometrical changes, the N1−C2−C3−C4 torsional angle and the puckering amplitude show significant parallel variations with the computational level. Thus, for the equatorial conformer, the N−C−C−C torsion takes values as 27.72°(MP2) > 27.09°(QCISD) > 26.43°(CISD) > 26.20°(B3LYP) > 25.44°(HF), and the puckering amplitudes q are 0.452(MP2) > 0.442(QCISD) > 0.429(CISD) > 0.428(B3LYP) > 0.413(HF). This trend is observed for both axial and equatorial forms (see Tables 1 and 3). According to the previous, the C−N bond lengthening caused by the inclusion of electron correlation explains why the geometry of the pyrrolidine ring is predicted to be more puckered with correlated methods. On the other hand, the puckering amplitudes confirm that the equatorial structure is always more puckered than the axial conformation. This geometrical feature makes more favorable the hyperconjugative interaction between the trans C−H bonds and the nitrogen lone pair in the equatorial conformer and explains why the C2−H8 bond lengths are significantly longer than the C2−H7 ones.[35]

The experimental geometrical parameters included in Table 3 correspond to the r_a electron diffraction results obtained by Caminati et al.[7] The electron diffraction data were interpreted with the help of some assumptions based on HF/4-21G(N*) calculations: equal C−C bond lengths, equal C−H bonds lengths, equal H−C−H angles, CH_2 groups with local C_{2v} symmetry, and a fixed position for the hydrogen bonded to the nitrogen. With these assumptions, only six geometrical parameters were refined in the least-squares analysis of the data. It was also outlined that the experimental radial distribution was not very sensitive to the conformation, and only peaks for r > 2.7 Å changed slightly when several conformations were considered in the electron diffraction analysis. The attempts to reduce the error limits of the experimental geometries by using the available microwave data had to be abandoned because of the low-frequency puckering vibration. Despite these experimental difficulties, on the basis of the preference for the axial form predicted at the HF/4-21G(N*) level, the electron diffraction data were interpreted in terms of the axial conformer.[7]

In light of the theoretical results presented above, a reinterpretation of the experimental conclusions seems convenient, because no further analysis of the electron diffraction data was made after finding that the equatorial form is more stable. It must be kept in mind that a direct comparison between ab initio calculations and electron diffraction data might be not strictly meaningful because the calculated parameters correspond to equilibrium geometries (r_e), and the electron diffraction data (r_a and r_g) represent a thermal average over vibrational positions.[36] In contrast to this asseveration, it has been recently suggested that B3LYP/6-31G** bond lengths can directly represent r_g values.[37] On comparing experiment and theory, some points deserve special attention. Thus, the experimental N−H bond length (1.020 Å) and C−N−H angle (107.0°) were taken from the ab initio HF/4-21G(N*) geometry of the axial form. However, our computations show that the C−N−H angle take values that differ by about 4° between the N−H axial and equatorial conformer. Moreover, the experimental dependent N−C−C parameter (104.6°) is an average between the computed angles in the axial and equatorial forms (around 107° and 102°, respectively). These geometrical features and the experimental difficulties mentioned above suggest that there might be some uncertainty in the experimental results. In agreement with this idea, a detailed observation of the data in Table 3 shows that the computed geometrical parameters for *both* the axial and equatorial forms take values within the error limits of the experimental results. Therefore, a definitive conclusion about the conformational preference at the N−H position from electron diffraction data cannot be obtained, because *both* axial and equatorial structures of PYR could be compatible with the available electron diffraction results.

The theoretical rotational constants for the axial and equatorial conformers are in good agreement with the experimental data[6,8]

TABLE 4: Theoretical and Experimental Rotational Constants, Imino Hydrogen (H6) Coordinates, Total Dipole Moments (μ_{tot}), and Dipole Components (in debyes) along the Principal Axes for the N−H Axial (E1) and Equatorial (E6) Conformers of Pyrrolidine

	rotational constants (MHz)			H6 coordinates (Å)						
	A	*B*	*C*	*k*	|*a*|	|*b*|	|*c*|	μ_{tot}	μ_a	μ_b	μ_c
					Experimental						
E1[6]	6834.536(5)	6677.844(11)	3888.063(1)	0.8936	1.3439	0.1505	1.2122		0.8	0.0	0.9 ± 0.4[8]
E6[8]	6864.678(5)	6791.950(5)	3902.3(20)	0.9509	2.13(4)	0.0	0.1(2)		0.4	0.0	1.0 ± 0.4[8]
					HF/6-31G**						
E1	6905.91	6761.95	3915.94	0.9037	1.3448	0.0000	1.1968	1.43	1.22	0.00	0.75
E6	6934.07	6872.19	3919.06	0.9589	2.1138	0.0000	0.0251	1.05	0.02	0.00	1.05
					MP2/6-31G**						
E1	6903.15	6711.34	3922.34	0.8713	1.2722	0.0000	1.2350	1.41	1.34	0.00	0.42
T1	6906.48	6713.20	3926.20	0.8703	1.2937	0.0625	1.2204	1.41	1.23	0.04	0.69
E6	6925.60	6849.50	3945.17	0.9489	2.1205	0.0000	0.0314	1.14	0.24	0.00	1.11
					B3LYP/6-31G**						
E1	6828.54	6643.08	3863.85	0.8749	1.3254	0.0000	1.2204	1.31	1.10	0.00	0.72
E6	6844.45	6782.63	3880.52	0.9583	2.1318	0.0000	0.0146	0.93	0.03	0.00	0.93
					QCISD/6-31G**						
E1	6865.31	6689.04	3894.83	0.8813	1.2961	0.0000	1.2251	1.42	1.35	0.00	0.44
E6	6891.44	6814.71	3914.86	0.9484	2.1217	0.0000	0.0126	1.06	0.23	0.00	1.04
					CISD/6-31G**						
E1	6933.03	6768.39	3935.46	0.8901	1.3074	0.0000	1.2134	1.43	1.35	0.00	0.47
E6	6960.86	6890.35	3946.48	0.9532	2.1139	0.0000	0.0255	1.05	0.23	0.00	1.02

[a] Asymmetry parameter $k = (2B - A - C)/(A - C)$.

displayed in Table 4. Except for B3LYP, the computed rotational constants are somewhat larger than the experimental values. The best numerical agreement corresponds to the QCISD and B3LYP calculations, with mean deviations of 18 and 19 MHz with respect to the experimental values. The computed coordinates of the H6 amino hydrogen also agree notably with the experimental r_s coordinates. This correspondence between experimental and theoretical data reinforces the assignment proposed by Caminati et al. for the conventional microwave and the millimeter wave free jet spectra to the axial and equatorial conformers, respectively.[6,8] Caminati et al. also outlined that the missed observation of the equatorial conformer in the conventional microwave spectrum could be due to the small value of the μ_a dipole moment component. The "experimental" dipole components along the principal axes shown in Table 4 correspond to their estimations by vectorial composition of bond dipole moments, and were used to obtain the approximate value of 220 cm^{-1} for the axial−equatorial energy difference from the jet experiment.[8] The theoretical dipole components confirm the small values of the μ_a dipole component (between 0.24 and 0.02 D) for the equatorial form. However, the large uncertainties in the "experimental" dipole components and the discrepancies between the experimental and theoretical values suggest that the proposed energy difference of 220 cm^{-1} can be somehow unreliable.

With regard to vibrational data, Geidel et al.[10] reported recently the infrarred and Raman spectra of PYR and its deuterated isotope at the N−H position. The authors also presented an assignment of the vibrational frequencies to normal modes coordinates and computed the HF/6-31G*, MP2/6-31G* and B3LYP/6-31G* scaled quantum mechanical (SQM) force fields. Both the assignment and the force field calculations were performed on the basis of the structure and frequencies of the axial form, which was predicted to be more stable with the 6-31G* basis set. In light of the results discussed above, which indicated that the equatorial form is definitively the most stable conformer, we have performed a new vibrational assignment on the basis of the calculated spectrum of the equatorial conformer. For this purpose, the 36 normal vibrational modes have been expressed in terms of symmetry coordinates[31] (Table 5), divided into two groups of 19 A′ and 17 A″ symmetries. Our symmetry coordinates are different from the internal coordinates of Geidel et al., where all C−H stretching and C−H deformation vibrations were labeled together in the normal-mode analysis as νCH and δCH, respectively.[10] The HF/6-31G**, MP2/6-31G**, and B3LYP/6-31G** SQM force fields have been obtained by applying the sets of optimized scaling factors shown in Table 6. Because of the characteristic large amplitude motion of the pseudorotational deformation mode, the force constant associated to this symmetry coordinate was not included in the fitting.[3e] The scale factors have been chosen as a compromise between a relatively small number of parameters with physical significance and a good fitting to the experimental frequencies. Furthermore, the number of parameters is small enough so that they could be transferred to structurally similar compounds.[30] Both the vibrational frequencies of PYR and its N−D isotope were employed in the fitting.

Experimental and SQM computed vibrational spectra are shown in Table 7. For the sake of comparison, we also included the unscaled ab initio frequencies and the "fixed scaled frequencies" obtained by multiplying the HF, MP2, and B3LYP harmonic frequencies by factors of 0.89, 0.95, and 0.96, respectively. It can be observed that scaling the force constants with multiple scale factors yields better results than the direct scaling of the computed frequencies. Thus, the SQM force fields reproduce the experimental frequencies of both PYR and its N−D isotopomer with total root-mean-square errors of 23.0, 23.1, and 20.4 cm^{-1} at the HF/6-31G**, B3LYP/6-31G**, and MP2/6-31G** levels, respectively. The largest deviations between experimental and theoretical frequencies take values around 70 cm^{-1} and correspond in all of the cases to bands assigned to extensively mixed vibrational motions. The vibrational frequencies of PYR and its N−D isotopomer were interpreted by using the SQM MP2/6-31G** potential energy distribution, which seems to compare slightly better with the experiment. This assignment was found to be nearly the same

TABLE 5: Definition of Symmetry Coordinates[31] for Pyrrolidine

coordinates	symmetry	description
$S_1 = r_{H6-N1}$	A′	N−H stretch
$S_2 = r_{H7-C2} + r_{H8-C2} + r_{H13-C5} + r_{H14-C5}$	A′	$\alpha(CH_2)$ sym stretch
$S_3 = r_{H7-C2} - r_{H8-C2} + r_{H13-C5} - r_{H14-C5}$	A′	$\alpha(CH_2)$ asym stretch
$S_4 = r_{H9-C3} + r_{H10-C3} + r_{H11-C4} + r_{H12-C4}$	A′	$b(CH_2)$ sym stretch
$S_5 = r_{H9-C3} - r_{H10-C3} + r_{H11-C4} - r_{H12-C4}$	A′	$b(CH_2)$ asym stretch
$S_6 = \theta_{H8-C2-H7} + \theta_{H14-C5-H13}$	A′	$\alpha(CH_2)$ sym bend
$S_7 = \theta_{H10-C3-H9} + \theta_{H12-C14-H11}$	A′	$b(CH_2)$ sym bend
$S_8 = \theta_{H7-C2-N1} - \theta_{H7-C2-C3} + \theta_{H8-C2-N1} - \theta_{H8-C2-C3} + \theta_{H13-C5-N1} - \theta_{H13-C5-C4} + \theta_{H14-C5-N1} - \theta_{H14-C5-C4}$	A′	$\alpha(CH_2)$ sym wag
$S_9 = \theta_{H9-C3-C2} - \theta_{H9-C3-C4} + \theta_{H10-C3-C2} - \theta_{H10-C3-C4} + \theta_{H11-C4-C5} - \theta_{H11-C4-C3} + \theta_{H12-C4-C5} - \theta_{H12-C4-C3}$	A′	$\beta(CH_2)$ sym wag
$S_{10} = \theta_{H7-C2-N1} - \theta_{H7-C2-C3} - \theta_{H8-C2-N1} + \theta_{H8-C2-C3} + \theta_{H13-C5-N1} - \theta_{H13-C5-C4} - \theta_{H14-C5-N1} + \theta_{H14-C5-C4}$	A′	$\alpha(CH_2)$ sym twist
$S_{11} = \theta_{H9-C3-C2} - \theta_{H9-C3-C4} - \theta_{H10-C3-C2} + \theta_{H10-C3-C4} + \theta_{H11-C4-C5} - \theta_{H11-C4-C3} - \theta_{H12-C4-C5} + \theta_{H12-C4-C3}$	A′	$\beta(CH_2)$ sym twist
$S_{12} = \theta_{H7-C2-N1} + \theta_{H7-C2-C3} - \theta_{H8-C2-N1} - \theta_{H8-C2-C3} + \theta_{H13-C5-N1} + \theta_{H13-C5-C4} - \theta_{H14-C5-N1} - \theta_{H14-C5-C4}$	A′	$\alpha(CH_2)$ sym rock
$S_{13} = \theta_{H9-C3-C2} + \theta_{H9-C3-C4} - \theta_{H10-C3-C2} - \theta_{H10-C3-C4} + \theta_{H11-C4-C5} + \theta_{H11-C4-C3} - \theta_{H12-C4-C5} - \theta_{H12-C4-C3}$	A′	$\beta(CH_2)$ sym rock
$S_{14} = r_{C2-N1} + r_{C5-N1}$	A′	C−N sym stretch
$S_{15} = r_{C3-C2} + r_{C5-C4}$	A′	$C_\alpha C_\beta$ sym stretch
$S_{16} = r_{C4-C3}$	A′	$C_\beta C_\beta$ sym stretch
$S_{17} = \chi_{H6-C5-N1-C2}$	A′	N−H out of plane
$S_{18} = -0.80902(\theta_{N1-C2-C3} + \theta_{C4-C5-N1}) + 0.30902(\theta_{C2-C3-C4} + \theta_{C3-C4-C5}) + \theta_{C5-N1-C2}$	A′	ring bend
$S_{19} = 1.11803(\theta_{N1-C2-C3-C4} - \theta_{C3-C4-C5-N1}) + 1.80902(\theta_{C4-C5-N1-C2} - \theta_{C5-N1-C2-C3})$	A′	ring pucker
$S_{20} = r_{H7-C2} + r_{H8-C2} - r_{H13-C5} - r_{H14-C5}$	A″	$\alpha(CH_2)$ sym stretch
$S_{21} = r_{H7-C2} - r_{H8-C2} - r_{H13-C5} + r_{H14-C5}$	A″	$\alpha(CH_2)$ asym stretch
$S_{22} = r_{H9-C3} + r_{H10-C3} - r_{H11-C4} - r_{H12-C4}$	A″	$\beta(CH_2)$ sym stretch
$S_{23} = r_{H9-C3} - r_{H10-C3} - r_{H11-C4} + r_{H12-C4}$	A″	$\beta(CH_2)$ asym stretch
$S_{24} = \theta_{H6-N1-C2} - \theta_{H6-N1-C5}$	A″	N−H bend
$S_{25} = \theta_{H8-C2-H7} - \theta_{H14-C5-H13}$	A″	$\alpha(CH_2)$ asym bend
$S_{26} = \theta_{H10-C3-H9} - \theta_{H12-C14-H11}$	A″	$\beta(CH_2)$ asym bend
$S_{27} = \theta_{H7-C2-N1} - \theta_{H7-C2-C3} + \theta_{H8-C2-N1} - \theta_{H8-C2-C3} - \theta_{H13-C5-N1} + \theta_{H13-C5-C4} - \theta_{H14-C5-N1} + \theta_{H14-C5-C4}$	A″	$\alpha(CH_2)$ asym wag
$S_{28} = \theta_{H9-C3-C2} - \theta_{H9-C3-C4} + \theta_{H10-C3-C2} - \theta_{H10-C3-C4} - \theta_{H11-C4-C5} + \theta_{H11-C4-C3} - \theta_{H12-C4-C5} + \theta_{H12-C4-C3}$	A″	$\beta(CH_2)$ asym wag
$S_{29} = \theta_{H7-C2-N1} - \theta_{H7-C2-C3} - \theta_{H8-C2-N1} + \theta_{H8-C2-C3} - \theta_{H13-C5-N1} + \theta_{H13-C5-C4} + \theta_{H14-C5-N1} - \theta_{H14-C5-C4}$	A″	$\alpha(CH_2)$ asym twist
$S_{30} = \theta_{H9-C3-C2} - \theta_{H9-C3-C4} - \theta_{H10-C3-C2} + \theta_{H10-C3-C4} - \theta_{H11-C4-C5} + \theta_{H11-C4-C3} + \theta_{H12-C4-C5} - \theta_{H12-C4-C3}$	A″	$\beta(CH_2)$ asym twist
$S_{31} = \theta_{H7-C2-N1} + \theta_{H7-C2-C3} - \theta_{H8-C2-N1} - \theta_{H8-C2-C3} - \theta_{H13-C5-N1} - \theta_{H13-C5-C4} + \theta_{H14-C5-N1} + \theta_{H14-C5-C4}$	A″	α(CH2) asym rock
$S_{32} = \theta_{H9-C3-C2} + \theta_{H9-C3-C4} - \theta_{H10-C3-C2} - \theta_{H10-C3-C4} - \theta_{H11-C4-C5} - \theta_{H11-C4-C3} + \theta_{H12-C4-C5} + \theta_{H12-C4-C3}$	A″	$\beta(CH_2)$ asym rock
$S_{33} = r_{C2-N1} - r_{C5-N1}$	A″	C−N asym stretch
$S_{34} = r_{C3-C2} - r_{C5-C4}$	A″	$C_\alpha C_\beta$ asym stretch
$S_{35} = -1.11803(\theta_{N1-C2-C3} - \theta_{C4-C5-N1}) + 1.80902(\theta_{C2-C3-C4} - \theta_{C3-C4-C5})$	A″	ring bend
$S_{36} = -0.80902(\theta_{N1-C2-C3-C4} + \theta_{C3-C4-C5-N1}) + 0.30902(\theta_{C4-C5-N1-C2} + \theta_{C5-N1-C2-C3}) + \theta_{C2-C3-C4-C5}$	A″	ring pucker

TABLE 6: Optimized Scaling Factors Applied to the SQM Force Fields of Pyrrolidine Computed at Several Computational Levels with the 6-31G Basis Set**

coordinates[a]		HF	MP2	B3LYP
N−H stretching	($S_{1)}$	0.7903	0.8763	0.9115
C−H stretching	(S_2, S_3, S_4, S_5, S_{20}, S_{21}, S_{22}, S_{23})	0.8188	0.8465	0.9021
C−N stretching	(S_{14}, S_{33})	0.7211	0.8108	0.8542
C−C stretching	(S_{15}, S_{16}, S_{34})	0.7526	0.7619	0.8531
N−H bending	(S_{17}, S_{24})	0.6916	0.8439	0.8521
C−H bending	(S_6, S_7, S_8, S_9, S_{10}, S_{11}, S_{12}, S_{13}, S_{25}, S_{26}, S_{27}, S_{28}, S_{29}, S_{30}, S_{31}, S_{32})	0.7607	0.8552	0.8960
ring bending	(S_{18}, S_{19}, S_{35})	0.7636	0.9456	0.9207
ring pucker	(S_{36})[b]	1.0000	1.0000	1.0000

[a] See Table 5 for definition. [b] Pseudorotation vibrational mode left unscaled.

with the HF/6-31G** and B3LYP/6-31G** force fields, although small differences were observed in the sequence of the normal modes and the potential energy distribution of the strongly mixed CH_2 deformation modes.

The PED indicates that the highest frequency at 3356 cm^{-1} corresponds to a pure N−H stretching mode. Geidel et al.[10] reported the splitting of the N−H stretch absorption at 3356 cm^{-1} into two components (3350 and 3310 cm^{-1}) in the Raman spectrum of the liquid. It was suggested that the splitting is due to the presence of different conformers. Because the computed N−H frequency in the equatorial conformer was found to be always higher than in the axial form (3788 vs 3750, 3598 vs 3557, and 3527 vs 3481 cm^{-1} at the HF, MP2, and B3LYP, respectively), it is reasonable to assign the experimental Raman frequencies to the equatorial and axial forms, respectively.[38] This statement and the computed conformational preferences pre-

TABLE 7: Comparison between Experimental and Calculated Frequencies (in cm^{-1}) for the N−H Equatorial Conformer of Pyrrolidine and Its N-deuterated Isotopomer

	N−H											N−D				
	HF			MP2			B3LYP					SQM[c]				assignments (PED (%))[e]
	ab initio[a]	fixed[b]	SQM[c]	ab initio[a]	fixed[b]	SQM[c]	ab initio[a]	fixed[b]	SQM[c]	IR int[d]	exp[10]	HF	MP2	B3LYP	exp[10]	
A′	3788	3371	3368	3598	3418	3368	3528	3387	3368	0.47	3356	2465	2464	2464	2494	$100S_1$
A′	3269	2909	2958	3228	3067	2969	3128	3003	2970	48.03	2975	2958	2969	2970	2971	$98S_5$
A′	3238	2882	2929	3183	3024	2928	3086	2963	2931	11.33	2927	2929	2928	2931	2925	$62S_3$, $30S_2$
A′	3221	2867	2914	3163	3005	2910	3074	2951	2919	36.17	2889	2914	2910	2919	2873	$94S_4$
A′	3110	2768	2814	3040	2888	2797	2934	2817	2786	116.93	2824	2814	2797	2786	2816	$66S_2$, $33S_3$
A′	1671	1487	1457	1585	1506	1465	1548	1486	1465	0.79	1484	1457	1465	1464	1458	$79S_6$, $17S_7$
A′	1640	1460	1430	1560	1482	1443	1520	1459	1439	2.89	1447	1430	1442	1439	1440	$80S_7$, $17S_6$
A′	1539	1370	1339	1438	1366	1327	1408	1352	1329	3.24	1292	1334	1320	1324	1289	$78S_8$
A′	1448	1289	1263	1361	1293	1257	1325	1272	1254	1.22	1268	1262	1257	1254	1250	$59S_9$, $21S_{10}$
A′	1371	1220	1195	1281	1217	1187	1252	1202	1185	0.86	1211	1193	1185	1184	1193	$48S_{10}$, $18S_9$, $11S_{12}$
A′	1341	1193	1167	1263	1200	1167	1232	1183	1164	7.88	1181	1169	1162	1161	1174	$52S_{11}$, $13S_{12}$, $11S_9$
A′	1148	1022	997	1105	1050	1005	1070	1027	1002	0.58	974	993	996	995	951	$19S_{18}$, $17S_{16}$, $14S_{12}$, $14S_{15}$, $11S_{10}$
A′	1077	959	930	1035	983	949	1010	970	946	5.26	920	922	926	928	901	$27S_{12}$, $23S_{11}$, $17S_{17}$, $15S_{14}$
A′	1018	906	872	978	929	881	946	908	880	2.75	901	866	874	870	860	$45S_14$, $16S_{15}$, $13S_{11}$
A′	962	856	832	938	891	837	902	866	834	4.29	871	666	684	676	668	$31S_{17}$, $25S_{16}$, $19S_{14}$
A′	947	843	809	915	869	821	876	841	818	67.24	832	819	822	828	838	$47S_{15}$, $41S_{16}$
A′	830	739	717	791	751	729	768	737	722	24.08	789	757	776	770	720	$56S_{13}$, $18S_{17}$, $12S_{14}$
A′	621	553	536	591	561	561	579	556	549	41.18	579	471	503	484	501	$51S_{18}$, $24S_{17}$, $12S_{12}$
A′	301	268	263	314	298	304	297	285	285	4.49	299	253	293	274	292	$84S_{19}$
A″	3247	2890	2937	3210	3050	2953	3108	2984	2951	0.60	2967	2937	2953	2951	2971	$96S_{23}$
A″	3229	2874	2922	3180	3021	2925	3078	2955	2923	56.01	2916	2922	2925	2923	2925	$65S_{21}$, $30S_{20}$
A″	3208	2855	2903	3154	2996	2902	3068	2945	2914	16.94	2879	2903	2902	2914	2873	$98S_{22}$
A″	3102	2761	2807	3038	2886	2795	2928	2811	2780	38.16	2818	2807	2795	2780	2816	$67S_{20}$, $32S_{21}$
A″	1653	1471	1441	1567	1489	1449	1528	1467	1447	2.41	1459	1441	1449	1446	1447	$92S_{25}$
A″	1616	1438	1409	1538	1461	1421	1500	1440	1420	0.54	1412	1409	1421	1420	1415	$93S_{26}$
A″	1582	1408	1345	1463	1390	1342	1443	1385	1344	3.59	1341	784	795	795	797	$53S_{24}$, $29S_{27}$
A″	1460	1299	1267	1362	1294	1258	1334	1281	1259	11.68	1273	1305	1291	1293	1289	$41S_{28}$, $22S_{30}$, $16S_{24}$
A″	1441	1282	1248	1336	1269	1234	1313	1260	1240	12.48	1228	1262	1239	1251	1233	$40S_{28}$, $38S_{27}$
A″	1366	1216	1188	1279	1215	1182	1252	1202	1183	8.59	1203	1211	1211	1213	1206	$55S_{30}$, $11S_{27}$
A″	1319	1174	1149	1230	1169	1136	1205	1157	1138	1.06	1171	1165	1155	1160	1153	$57S_{29}$, $15S_{27}$
A″	1239	1103	1078	1164	1106	1067	1139	1093	1074	9.89	1099	1074	1062	1072	1038	$44S_{31}$, $21S_{33}$, $13S_{32}$, $10S_{29}$
A″	1202	1070	1031	1133	1076	1038	1110	1066	1036	0.32	1023	1116	1104	1095	1107	$45S_{33}$, $20S_{32}$
A″	998	888	863	968	920	856	933	896	865	0.13	883	924	927	932	918	$74S_{34}$, $11S_{33}$
A″	941	837	819	895	850	831	876	841	828	2.51	848	831	832	833	848	$33S_{32}$, $29S_{31}$, $12S_{33}$
A″	686	611	599	635	603	606	638	612	609	0.65	600	596	603	606	601	$61S_{35}$, $13S_{31}$
A″	62	55	62	66	63	65	79	76	79	0.18	65	62	65	79	65	$60S_{36}$, $20S_{32}$, $12S_{34}$
rms[f]	209.80	36.70	24.49	146.58	55.12	21.74	94.74	29.97	24.35			21.60	19.04	21.93		
max[g]	432	78	72	275	117	60	189	66	67			45	56	50		

[a] Unscaled computed vibrational frequencies obtained with the 6-31G** basis set. [b] Fixed scaled ab initio frequencies with factors of 0.89, 0.95, and 0.96 at the HF, MP2, and B3LYP levels, respectively. [c] Scaled quantum mechanical vibrational frequencies. [d] Calculated intensities in km/mol at the MP2/6-31G** level. [e] Obtained with the SQM MP2/6-31G** force field. Contributions less than 10% are omitted. [f] Root-mean-square deviation in cm^{-1}. [g] Maximum deviation (cm^{-1}) between experimental and theoretical frequencies.

sented above confirm that the experimental frequencies shown in Table 7 must be assigned to the equatorial conformer and not to the axial one. It can be also noted that the N−H stretching band is shifted to 2494 cm^{-1} by deuteration.

According to the description of the normal modes in the C−H region between 2800 and 3000 cm^{-1}, no mixing is observed between $\alpha(CH_2)$ and $\beta(CH_2)$ stretching modes. Furthermore, the vibrational assignment shows that the $\beta(CH_2)$ stretching vibrations show higher frequencies than the $\alpha(CH_2)$. This assignment also allows us to interpret the C−H stretching bands of PYR and deuterated derivatives reported by Krueger and Jan.[39a] On the basis of our calculated intensities (Table 7) and the infrared spectrum depicted in ref 39a, the two intense bands around 2962 and 2872 cm^{-1} would correspond to the 2975 and 2889 cm^{-1} ones in the IR spectrum of Geidel et al.[10] These two bands, almost unchanged by α-d_2 and α,α'-d_4 deuteration, were interpreted by Krueger and Jan as "normal" asymmetric and symmetric CH_2 stretching vibrations.[39a] According to the PED in Table 7, these bands are assigned to the A′ asymmetric and A′ symmetric $\beta(CH_2)$ stretching vibrations, respectively. On the other hand, Krueger and Jan reported a shoulder at 2930 and a band at 2821 cm^{-1},[39a] which were interpreted as the asymmetric and symmetric vibrations of a "perturbed" $\alpha(CH_2)$ group by the presence of the lone pair of the nitrogen.[39b] Both bands disappear in the α,α'-d_4 deuterated compound. According to our calculations, these signals correspond approximately with the bands at 2916 and 2824 cm^{-1} by Geidel et al.[10] and can be assigned to the A″ asymmetric and the A′ symmetric $\alpha(CH_2)$ stretching, respectively. Finally, it must be also noted that Geidel et al. pointed out that the highest C−H stretching wavenumbers (2975 and 2967 cm^{-1}) correspond to $\alpha(CH_2)$ groups.[10] According to the results presented here, this assignment is unsatisfactory, probably because the frequencies of the axial conformer were used for their vibrational analysis.

With regard to the N−H deformation modes, different assignments have been proposed in the literature. Evans et al.[4b] assigned the bands at 1418 and 792 cm^{-1} to the N−H bending and the N−H out-of-plane deformation, respectively. McCullough et al.[4c] assigned a frequency of 990 cm^{-1} to the N−H out-of-plane motion. Geidel et al.[10] proposed the bands at 1341 and 832 cm^{-1}, shifted to 1193 and 668 cm^{-1} by deuteration, for the A″ and A′ N−H bendings, respectively. On the basis of

the PED in Table 7, a different assignment can be proposed. Thus, the band at 1341 cm^{-1} is assigned to the A″ N−H bending, although with considerable mixing with $\alpha(CH_2)$ motions. However, our calculations indicate that this band is remarkably shifted to 797 cm^{-1} by deuteration. On the other hand, the A′ N−H out-of-plane vibration is extensively coupled with other normal modes and cannot be unambiguously assigned. Thus, the bands at 920, 871, 789, and 579 cm^{-1} show a contribution of around 20% of this N−H deformation. These bands are shifted to 901, 668, 720, and 501 cm^{-1} in the deuterated compound.

The rest of the spectrum is dominated by CH_2 and ring deformation modes. The bands between 1412 and 1484 cm^{-1} can be assigned to the CH_2 bending vibrations, which are the only ones clearly separated from the rest of deformation motions. In contrast to the stretching vibrations, the $\alpha(CH_2)$ bendings have higher frequencies than the $\beta(CH_2)$ ones. The bands between 1300 and 600 cm^{-1} can be assigned to ring-bond stretchings and very mixed vibrations with contributions of CH_2 wagging, twisting, and rocking modes. The vibrational motions with larger contributions from ring-bond stretching modes appear at lower frequencies, and according to the PED, the C−N and C−C stretching motions appear to be almost unmixed. An analogous trend has been reported for tetrahydrofuran.[2d,2e] The four last bands correspond to ring deformation modes. Thus, the bands at 600 and 579 cm^{-1} are assigned to the A′ and A″ ring-bending modes mixed with N−H and CH_2 motions, and the band at 299 corresponds to an almost pure ring puckering vibration. The lowest frequency at 65 cm^{-1} should be assigned to the large amplitude motion of pseudorotation governing the interconversion between the axial and equatorial conformers.

Conclusions

The conformational stabilities of pyrrolidine have been definitively established by using ab initio calculations. In agreement with the last experimental data available, the N−H equatorial envelope conformer was found to be more stable than the N−H axial one. The best theoretical estimate for the axial−equatorial energy difference is about 80−100 cm^{-1}, somewhat lower than the experimental value of around 220 cm^{-1} given by Caminati et al.[8] Both stable conformers may interchange by pseudorotation, a process with an energy barrier around 150 cm^{-1}. This process is clearly more favorable than the interconversion through the planar form, because this structure was found to be at least 1500 cm^{-1} less stable than the envelope conformations.

Basis set dependencies and electron correlation effects have been analyzed. According to the results presented, the use of large basis sets is essential for a correct description of the conformational energies. Thus, HF and CISD computations predicted the correct equatorial preference with all of the basis sets employed. However, contradictory results were obtained when basis sets of moderate size were used with perturbative electron correlation methods (MP2, QCI, and CC) and density functional methods. The electron correlation effects are concentrated on the reduction of the axial−equatorial energy difference and of the height of the pseudorotational barrier.

In light of the theoretical results obtained, the reported electron diffraction geometries and rotational constants have been reinterpreted. It was found that the computed geometries for both the axial and equatorial forms can be compatible with the electron diffraction data. The theoretical rotational constants of the axial and equatorial conformers were in good agreement with the data obtained by conventional microwave and free jet millimeter wave experiments, respectively.

A detailed reassignment of the experimental vibrational frequencies for pyrrolidine and its N−D isotopomer has been performed. The theoretical frequencies obtained for the equatorial conformer using several scaled quantum mechanical force fields reproduced adequately the experimental data. New assignments for the bands in the C−H stretching region have been given, which also allows a proper interpretation of the experiments of Krueger et al.[39] On the other hand, although the A″ N−H bending can be unambiguously assigned to the experimental band at 1341 cm^{-1}, the A′ N−H out of plane motion is strongly mixed with CH_2 vibrations.

Acknowledgment. L.C. and I.P.J. are indebted to the Xunta de Galicia and to the University of Vigo for financial support. I.P.J. gratefully acknowledges the Flemish Science Foundation (FWO-Vlaanderen) for an appointment as Visiting Postdoctoral Fellow.

References and Notes

(1) (a) Laane, J. Pseudorotation of Five-Membered Rings. In *Vibrational Spectra and Structure*; Durig, J. R., Ed.; Marcel Dekker: New York, 1972; Vol 1. (b) Legon, A. C. *Chem. Rev.* **1980**, *80*, 231. (c) Strauss, H. L. *Annu. Rev. Phys. Chem.* **1983**, *34*, 310.

(2) (a) Kilpatrick, J. E.; Pitzer, K. S.; Spitzer, R. *J. Am. Chem. Soc.* **1947**, *69*, 2483. (b) McCullough, J. P.; Pennington, R. E.; Smith, J. C.; Hossenlopp, I. A.; Waddington, G. *J. Am. Chem. Soc.* **1959**, *81*, 5880. (c) Adams, W. J.; Geise, H. J.; Bartell, L. S. *J. Am. Chem. Soc.* **1970**, *92*, 5013. (d) Cadioli, B.; Gallinella, E.; Coulombeau, C.; Jobic, H.; Berthier, G. *J. Phys. Chem.* **1993**, *97*, 7844. (e) Strajbl, M.; Baumruk, V.; Florian, J. *J. Phys. Chem. B* **1998**, *102*, 1314.

(3) (a) Cremer D.; Pople, J. A. *J. Am. Chem. Soc.* **1975**, *97*, 1358. (b) Cremer D.; Pople, J. A. *J. Am. Chem. Soc.* **1975**, *97*, 1354. (c) Cremer, D. *Isr. J. Chem.* **1980**, *20*, 12. (d) Cremer, D. *J. Phys. Chem.* **1990**, *94*, 5502.

(4) (a) Hildenbrand, D. L.; Sinke, G. C.; McDonald, R. A.; Kramer, W. R.; Stull, D. R. *J. Chem. Phys.* **1959**, *31*, 650. (b) Evans, J. C.; Wahr, J. C. *J. Chem. Phys.* **1959**, *31*, 655. (c) McCullough, J. P.; Douslin, D. R.; Hubbard, W. N., Todd, S. S.; Messerly, J. F.; Hossenlopp, I. A.; Frow, F. R.; Dawson, J. P.; Waddington, G. *J. Am. Chem. Soc.* **1959**, *81*, 5884.

(5) (a) Pitzer, K. S.; Donath, W. E. *J. Am. Chem. Soc.* **1959**, *81*, 3213. (b) Baldock, R. W.; Katritzky, A. R. *J. Chem. Soc. B* **1968**, 1470. (c) Krueger, P. J.; Jan, J. *Can. J. Chem.* **1970**, *48*, 3236. (d) Lambert, J. B.; Oliver, W. L., Jr. *J. Am. Chem. Soc.* **1969**, *91*, 7774. (e) Lambert, J. B.; Papay, J. J.; Magyar, E. S.; Neuberg, M. K. *J. Am. Chem. Soc.* **1973**, *95*, 4458. (f) Breuer, E.; Melumad, D. *J. Org. Chem.* **1973**, *38*, 1601. (g) Lambert, J. B.; Papay, J. J.; Khan, S. A.; Kappauf, K. A.; Magyar, E. S. *J. Am. Chem. Soc.* **1974**, *96*, 6112. (h) Duthaler, R. O.; Williamson, K. L.; Giannini, D. D.; Bearden, W. H.; Roberts, J. D. *J. Am. Chem. Soc.* **1977**, *99*, 8406.

(6) Caminati, W.; Oberhammer, H.; Pfafferott, G.; Filgueira, R. R.; Gomez, C. H. *J. Mol. Spectrosc.* **1984**, *106*, 217.

(7) Pfafferott, G.; Oberhammer, H.; Boggs J. E.; Caminati, W. *J. Am. Chem. Soc.* **1985**, *107*, 2305.

(8) Caminati, W.; Dell'Erba, A.; Maccaferri, G.; Favero, P. G. *J. Mol. Spectrosc.* **1998**, *191*, 45.

(9) Han, S. J.; Kang, Y. K. *THEOCHEM* **1996**, *362*, 243.

(10) Billes, F.; Geidel, E. *Spectrochim. Acta Part A* **1997**, *53*, 2537.

(11) Carballeira, L.; Pérez-Juste, I. *J. Chem. Soc., Perkin Trans. 2* **1998**, 1339.

(12) Strajbl, M.; Florian, J. *Theor. Chem. Acc.* **1998**, *99*, 166.

(13) Pulay, P. *Mol. Phys.* **1970**, *18*, 473

(14) Frisch, M. J.; Trucks, G. W.; Schlegel, H. B.; Gill, P. M. W.; Johnson, B. G.; Robb, M. A.; Cheeseman, J. R.; Keith, T.; Petersson, G. A.; Montgomery, J. A.; Raghavachari, K.; Al-Laham, M. A.; Zakrzewski, V. G.; Ortiz, J. V.; Foresman, J. B.; Cioslowski, J.; Stefanov, B. B.; Nanayakkara, A.; Challacombe, M.; Peng, C. Y.; Ayala, P. Y.; Chen, W.; Wong, M. W.; Andres, J. L.; Replogle, E. S.; Gomperts, R.; Martin, R. L.; Fox, D. J.; Binkley, J. S.; Defrees, D. J.; Baker, J.; Stewart, J. P.; Head-Gordon, M.; Gonzalez, C.; Pople, J. A. *Gaussian 94*, revision B.2; Gaussian, Inc.: Pittsburgh, PA, 1995.

(15) Frisch, M. J.; Trucks, G. W.; Schlegel, H. B.; Scuseria, G. E.; Robb, M. A.; Cheeseman, J. R.; Zakrzewski, V. G.; Montgomery, J. A., Jr.; Stratmann, R. E.; Burant, J. C.; Dapprich, S.; Millam, J. M.; Daniels, A. D.; Kudin, K. N.; Strain, M. C.; Farkas, O.; Tomasi, J.; Barone, V.; Cossi, M.; Cammi, R.; Mennucci, B.; Pomelli, C.; Adamo, C.; Clifford, S.; Ochterski, J.; Petersson, G. A.; Ayala, P. Y.; Cui, Q.; Morokuma, K.; Malick, D. K.; Rabuck, A. D.; Raghavachari, K.; Foresman, J. B.; Cioslowski, J.;

Ortiz, J. V.; Stefanov, B. B.; Liu, G.; Liashenko, A.; Piskorz, P.; Komaromi, I.; Gomperts, R.; Martin, R. L.; Fox, D. J.; Keith, T.; Al-Laham, M. A.; Peng, C. Y.; Nanayakkara, A.; Gonzalez, C.; Challacombe, M.; Gill, P. M. W.; Johnson, B. G.; Chen, W.; Wong, M. W.; Andres, J. L.; Head-Gordon, M.; Replogle, E. S.; Pople, J. A. *Gaussian 98*, revision A.9; Gaussian, Inc.: Pittsburgh, PA, 1998.

(16) Møller, C.; Plesset, M. S. *Phys. Rev.* **1934**, *46*, 618.

(17) Raghavachari, K.; Pople, J. A. *Int. J. Quantum Chem.* **1981**, *20*, 167.

(18) Pople, J. A.; Head-Gordon, M.; Raghavachari, K. *J. Chem. Phys.* **1987**, *87*, 5968.

(19) Raghavachari, K. J.; Trucks, G. W.; Pople, J. A.; Head-Gordon, M.; *Chem. Phys. Lett.* **1989**, *157*, 479.

(20) Purvis, G. D.; Bartlett, R. J. *J. Chem. Phys.* **1982**, *76*, 1910.

(21) Becke, A. D. *Phys. Rev. A* **1988**, *38*, 3098.

(22) Vosko, S. H.; Wilk, L.; Nusair, M. *Can. J. Phys.* **1980**, *58*, 1200.

(23) Perdew, J. P.; Wang, X. *Phys. Rev. B* **1992**, *45*, 13244.

(24) Lee, C.; Yang, W.; Parr, R. G. *Phys. Rev. B* **1988**, *37*, 785.

(25) Becke, A. D. J. *Chem. Phys.* **1993**, *98*, 5648.

(26) Dunning, T. H.; Hay, P. J. *Modern Theoretical Chemistry*; Schaefer, H. F., III., Ed.; Plenum: New York, 1976.

(27) Clark, T.; Chandrasekhar, J.; Spitznagel, G. W.; Schleyer, P. v. R. *J. Comput. Chem.* **1983**, *4*, 294.

(28) Dunning, T. H. *J. Chem. Phys.* **1989**, *90*, 1007.

(29) Woon, D. E.; Dunning, T. H. *J. Chem. Phys.* **1993**, *98*, 1358.

(30) Pulay, P.; Fogarasi, G.; Pongor, F.; Boggs, J. E.; Vargha, A. *J. Am. Chem. Soc.* **1983**, *105*, 7037.

(31) Pulay, P.; Fogarasi, G.; Pang, F.; Boggs, J. E. *J. Am. Chem. Soc.* **1979**, *101*, 2550.

(32) Wilson, E. B.; Decius, J. C.; Cross, P. C. *Molecular Vibrations*; McGraw-Hill: New York, 1955.

(33) For the sake of clarity, the curves obtained with the 6-311G** basis set and the BVWN and BPW91 functionals, which were found to be very similar to those in Figure 2, are not included.

(34) One reviewer pointed out that the HF energies obtained with the 6-31G** and 6-311G** basis sets on the HF/6-31G** geometries are the most comparable values to the experimental one deduced from the microwave free jet experiment. However, it can be seen in Figure 3 that, for computations with less than 300 basis functions, the HF energies show large oscillations, and the axial form can be even predicted to be more stable if electron correlation is introduced. Furthermore, the experimental value of 220 cm^{-1} suggested by Caminati[8] should be considered as an upper limit for the axial−equatorial energy difference. According to all of the previous, we consider that the agreement between experiment and the HF/6-31G** and HF/6-311G** results is purely fortuitous.

(35) Because the use of large basis sets was found to be necessary for the correct prediction of conformational energies, HF, MP2, and B3LYP optimizations followed by computation of the vibrational frequencies have been also performed using the 6-311++G** basis set. For the sake of brevity, the results obtained were not included here, but it must be remarked that no significant differences were found with the 6-31G** results presented in Tables 3 and 7.

(36) Kuchitsu, K. *Accurate Molecular Structures. Their Determination and Importance*; Domenicano, A., Hargittai, I., Eds.; Oxford University Press: New York, 1992.

(37) Shishkov, I. F.; Shlykov, S.; Rousseau, B.; Peng, Z. H.; Van Alsenoy, C.; Geise, H. J.; Kataeva, O. N.; Herrebout, W. A.; Van der Veken, B. *J. Phys. Chem. A* **2001**, *105*, 1039.

(38) Dage, J.; Snavely, D. L.; Walters, V. A.; Office of Naval Res. N00014-K-0664, Technical Report No. 9, 1992.

(39) (a) Krueger, P. J.; Jan, J. *Can. J. Chem.* **1970**, *48*, 3229. (b) Bohlmann, F. *Chem. Ber.* **1958**, *91*, 2157.